ADVANCED FUNCTIONAL MATERIALS

Supporting Information

for *Adv. Funct. Mater.,* DOI: 10.1002/adfm.201501760

3D Printed Anatomical Nerve Regeneration Pathways

Blake N. Johnson, Karen Z. Lancaster, Gehua Zhen, Junyun He, Maneesh K. Gupta, Yong Lin Kong, Esteban A. Engel, Kellin D. Krick, Alex Ju, Fanben Meng, Lynn W. Enquist, Xiaofeng Jia, and Michael C. McAlpine**

Supporting Information

3D Printed Anatomical Nerve Regeneration Pathways

Blake N. Johnson, Karen Z. Lancaster, Gehua Zhen, Junyun He, Maneesh K. Gupta, Yong Lin Kong, Esteban A. Engel, Kellin D. Krick, Alex Ju, Fanben Meng, Lynn W. Enquist, Xiaofeng Jia[*], *Michael C. McAlpine*[*]

This Supporting Information includes: *in situ* scanning data obtained from intact tissue prior to transection as a proof-of-concept for future point-of-care applications; mechanical failure mechanisms observed during tensile strength measurements under both orientations of the printed material (with and against the grain); boundary conditions used for the mechanical finite element analysis studies; scanning electron micrograph showing the path along the luminal surface used in profilometry measurements; analysis of neurite networks and Schwann cell structures from control studies done in the absence of the 3D printed physical cue; growth of whole dorsal root ganglia on the 3D printed physical cue; a representative movie of the silicone nerve pathway printing process containing biochemical gradients; *in vitro* longitudinal imaging studies of axonal growth in 3D printed nerve guides; *in vivo* Schwann cell staining; a photograph of the 3D printing apparatus; and images of bifurcating nerve guide cross-sections.

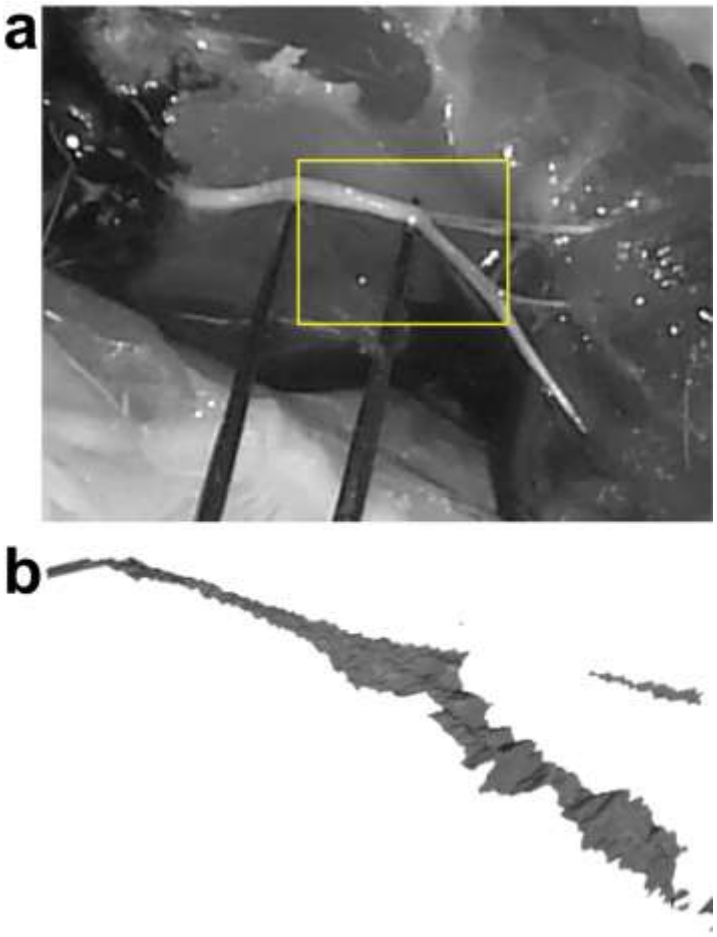

Figure S1. Scanning data obtained from intact tissue prior to transection as a proof-of-concept for *in situ* imaging applications. a) Photograph of the scanned sciatic nerve bifurcation (yellow box indicates the scanned region). b) Scan data obtained from *in situ* imaging.

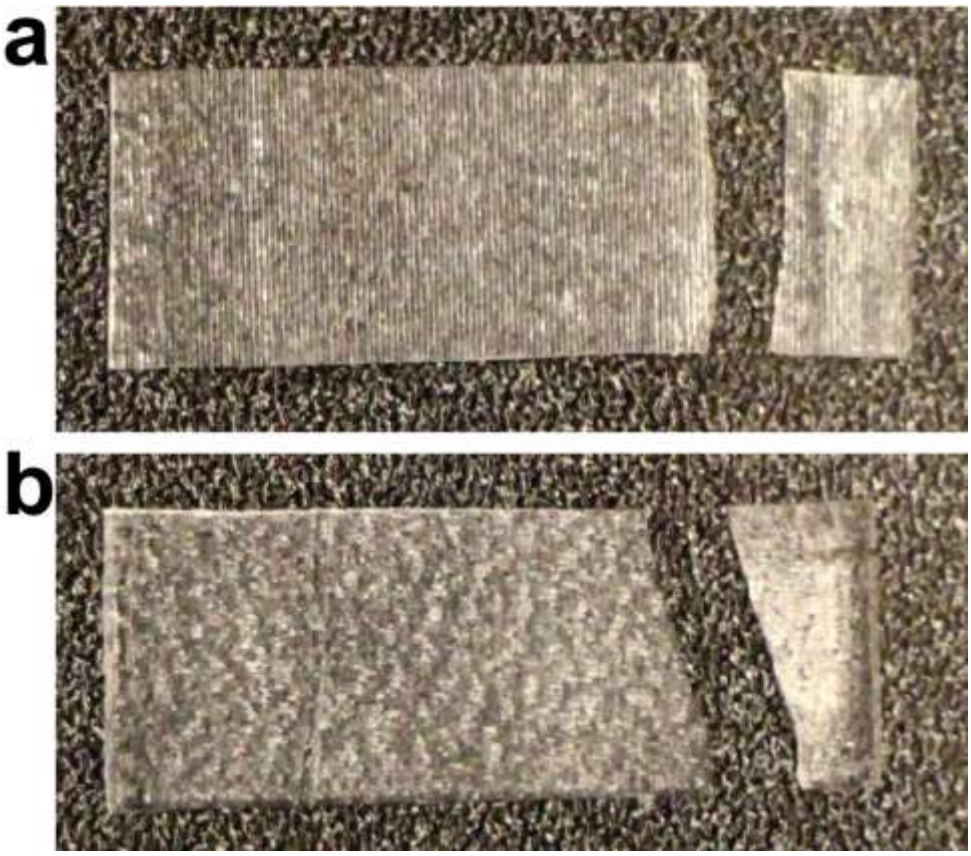

Figure S2. Mechanical failure mode observed during tensile strength measurements under various grain orientations of the printed material. a) Tear-based failure mechanism observed when the tensile load was applied against the 3D printed grain. b) Rip-based failure mechanism observed when the tensile load was applied with the 3D printed grain.

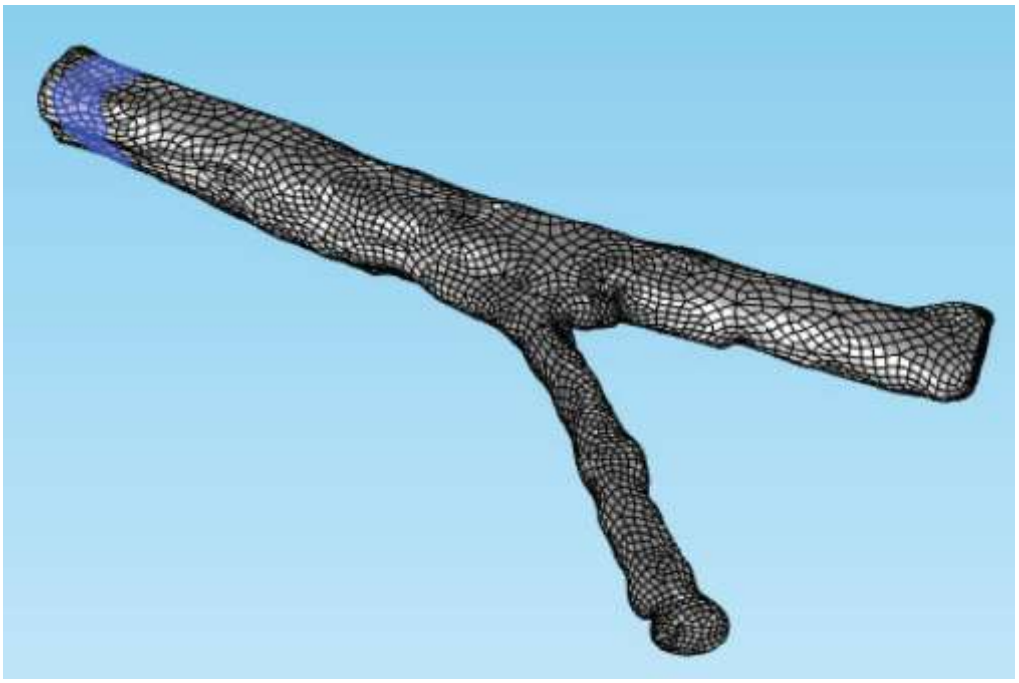

Figure S3. Boundary conditions used for mechanical finite element analysis studies. Blue highlighted elements were restricted to zero displacement condition; tensile and torsional loads were applied to the axial faces of the bifurcated distal end.

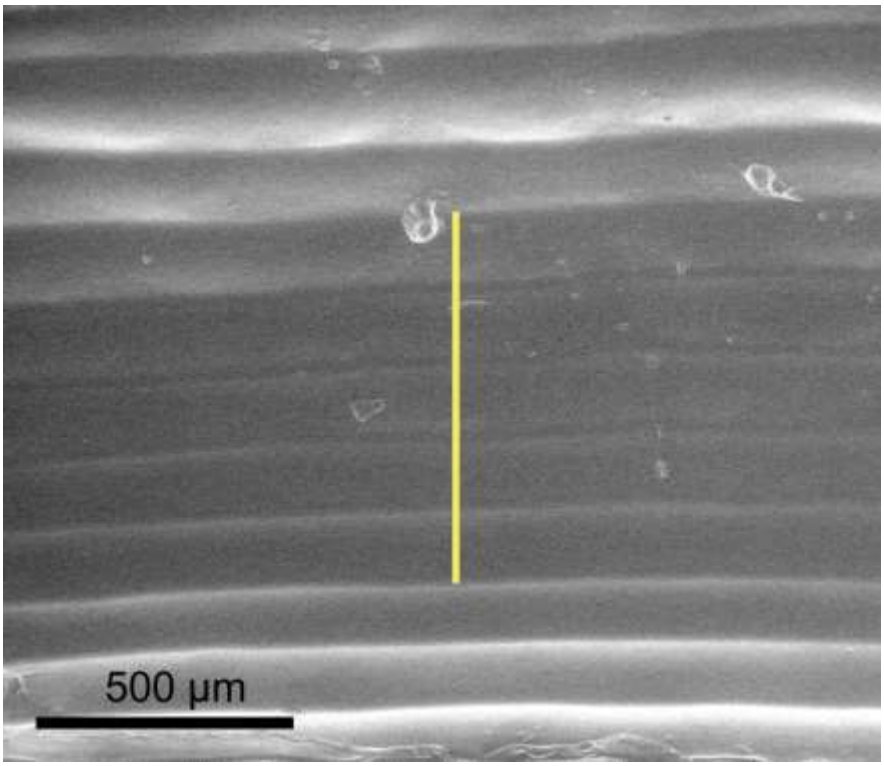

Figure S4. Scanning electron micrograph of the nerve regeneration pathway luminal surface. The image displays the profiled luminal surface corresponding to the profilometry measurement shown in Figure 4b. The yellow line indicates the path of the surface profiler.

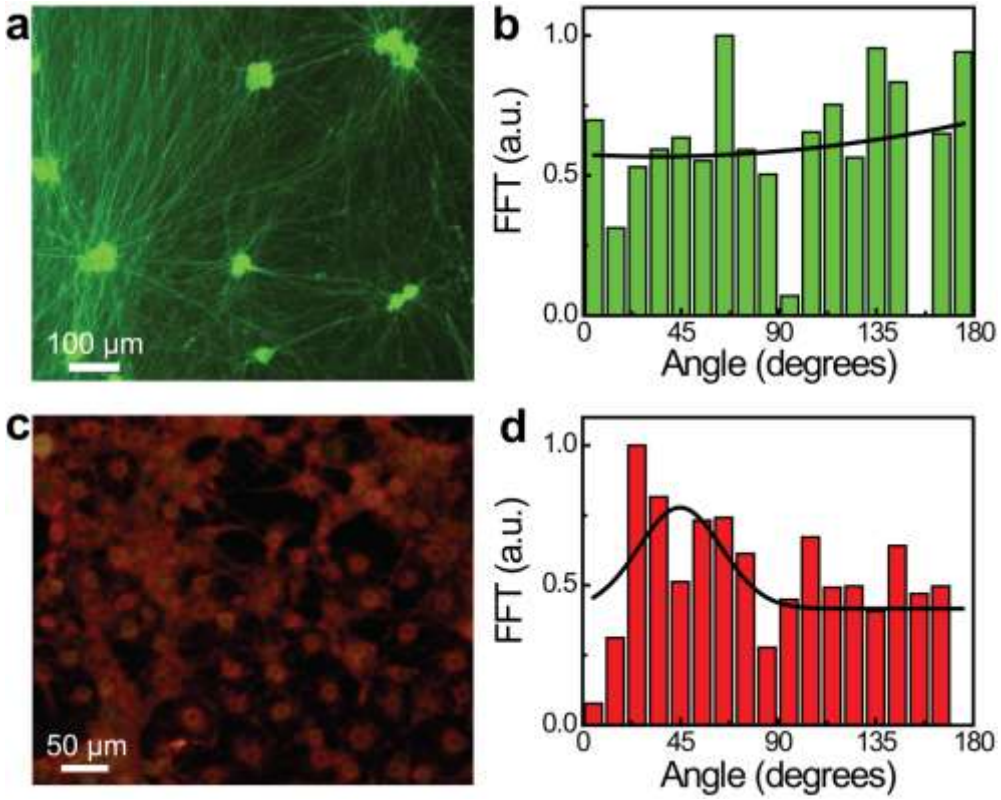

Figure S5. Analysis of the orientations of the neurite networks and Schwann cell structures from control studies done in the absence of the 3D printed physical cue. Neurite network structure (a) and corresponding orientation analysis (b) in the absence of the 3D printed physical cue. Schwann cell structure (c) and corresponding orientation analysis (d) in the absence of the 3D printed physical cue.

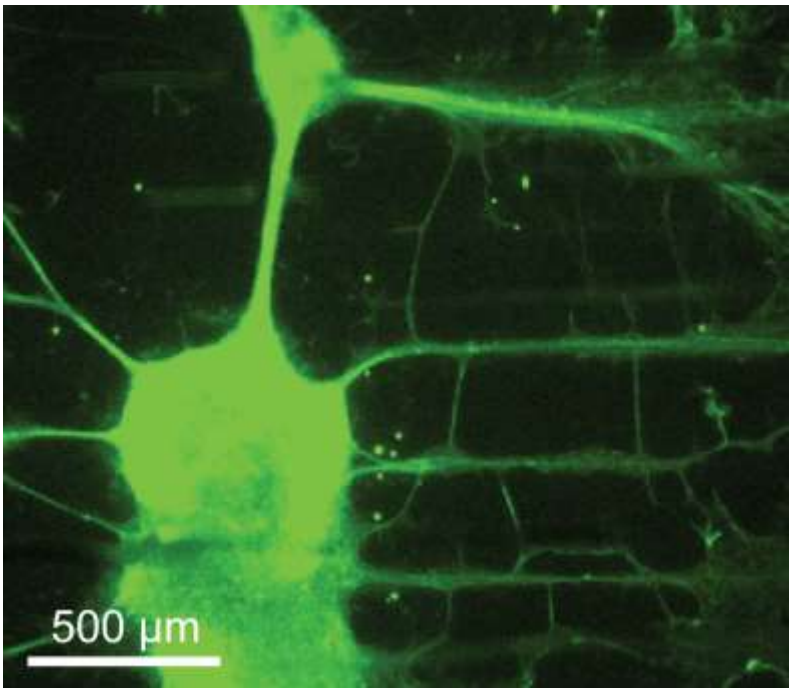

Figure S6. Growth of dorsal root ganglia on diced 3D printed nerve guides. The image shows neurite network alignment with the horizontally oriented physical cue.

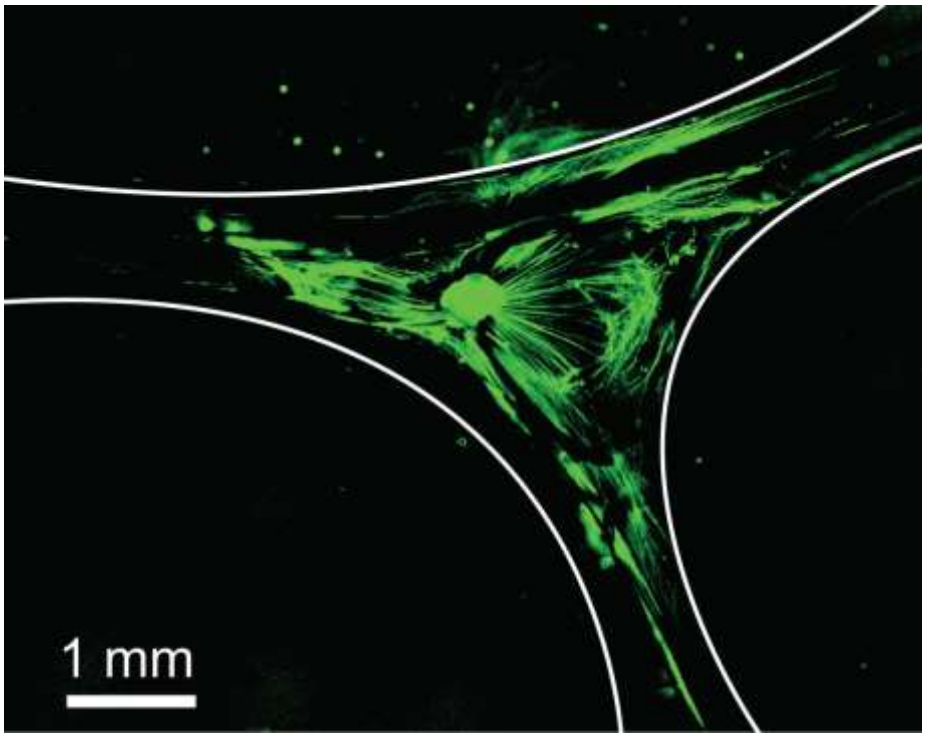

Figure S7. Tau staining of sensory axon outgrowth from dorsal root ganglia in a 3D printed bifurcating nerve guide.

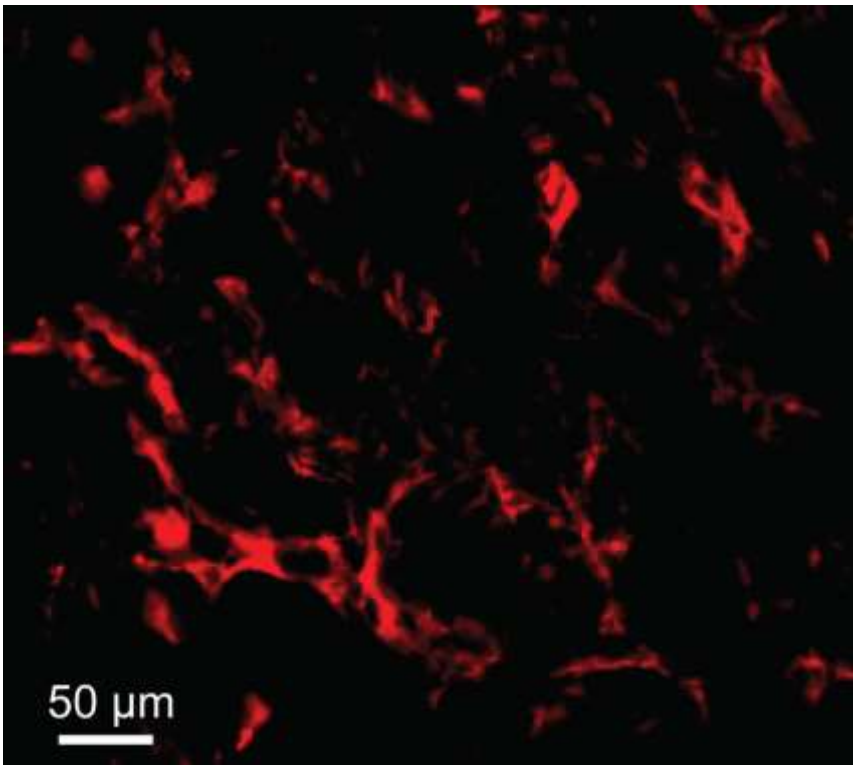

Figure S8. S100 staining of regenerated nerve reveals the presence of Schwann cells in both sensory and motor pathways (representative data from sensory pathway shown here).

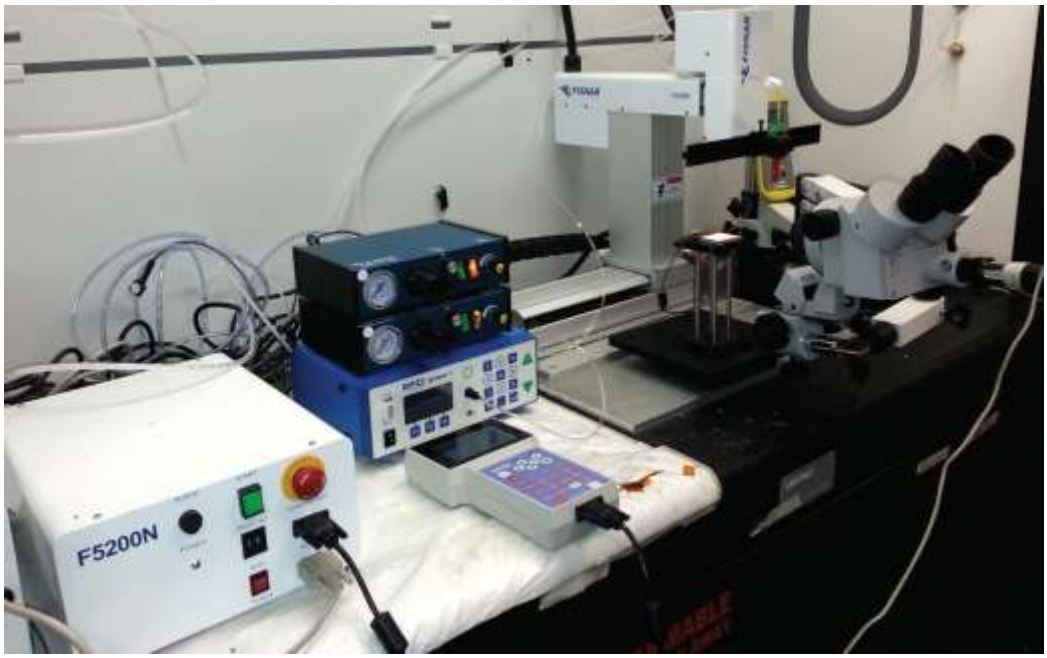

Figure S9. Photograph of the extrusion-based 3D printer highlighting the primary components, including the controller, the dispensing system, a three axes gantry robot, and a vision system.

Figure S10. Cross-sectional images of a 3D printed nerve guide at various positions along its length (L = 10 mm; positions from left to right correspond to L, 0.75L, distal bifurction region, proximal bifurcation region, 0.25L, and 0 mm).

Supporting Movie 1. Printing of a bifurcated silicone nerve pathway (scaffold printing × 32 speed; gradient printing × 16 speed).